Available online at www.sciencedirect.com
SCIENCE DIRECT®
International Journal of Heat and Fluid Flow 27 (2006) 65–79
International Journal of HEAT AND FLUID FLOW
www.elsevier.com/locate/ijhff

The structure of turbulence in a rod-roughened channel

Alireza Ashrafian [1], Helge I. Andersson *

Department of Energy and Process Engineering, Norwegian University of Science and Technology, N-7491 Trondheim, Norway

Received 4 September 2004; accepted 17 April 2005
Available online 21 July 2005

Abstract

This article is a sequel to the recent paper by Ashrafian et al. [Ashrafian, A., Andersson, H.I., Manhart, M., 2004. DNS of turbulent flow in a rod-roughened channel, International Journal of Heat and Fluid Flow 25, 373–383] on direct numerical simulation of a turbulent flow in a rod-roughened channel. Higher-order statistics are compared and the effects of surface roughness on the relatively large scales of the turbulent flow are investigated. It is observed that roughness tends to increase the intensity of the vorticity fluctuations in the roughness sublayer. In the outer layer, however, the r.m.s. of the vorticity fluctuations are unaffected. The Reynolds stress anisotropy invariant maps for the smooth and rough cases clearly showed that the states of near-wall turbulence for the two cases were substantially different whereas in the regions away from the wall the two cases exhibited close similarities. Differences in the turbulent transport process between the two cases were shown through examination of the third-order moments of the velocity fluctuations and the turbulent kinetic energy budgets. It was observed that wall-ward transport of the kinetic energy is substantially increased very close to the wall while the away-from-the-wall transport of kinetic energy is relatively reduced at the edge of the roughness sublayer. The length scales and flow dynamics in the roughness sublayer were also investigated. It was found that turbulence statistics and structure outside the roughness sublayer are hardly affected by the condition at the walls. These observations lent support to the classical wall similarity hypothesis.

Keywords: Turbulence structure; Channel flow; Rod roughness; DNS

1. Introduction

In wall turbulence, the no-slip condition induces a strong anisotropy of the flow field and leads to a mean-velocity gradient which, through the direct interaction with the turbulent momentum flux, provides the continuous source of turbulent kinetic energy necessary to maintain turbulence in the core of the flow (Jiménez and Pinelli, 1999). The action of wall roughness can be interpreted as an external forcing directly injecting turbulent energy in the flow field (Jiménez, 1999). Sufficiently high roughness elements destroy the autonomous cycle of turbulent kinetic energy production. Instead, some disrupted and unorganized structures take over the role of generating turbulence at the wall. That the conditions at a solid wall can globally determine the characteristics of turbulence is a possibility which may not be ignored. This is indeed opposite to Townsend's classical similarity hypothesis which assumes that "the turbulent flow in the outer layer is unlikely to be affected by the exact nature of the roughness and, as with a smooth wall, it will be determined only by the friction Reynolds number" (Townsend, 1976).

In the study of rough-wall boundary-layers, the classical theory has received substantial support through the experiments of Grass (1971) and Grass et al. (1993), the investigation of Perry et al. (1987), the comprehensive

* Corresponding author. Tel.: +47 73 59 35 56; fax: +47 73 59 34 91.
E-mail addresses: alireza.ashrafian@sintef.no (A. Ashrafian), helge.i.andersson@ntnu.no (H.I. Andersson).
[1] Address: Department of Process Technology Flow, Technology Team, SINTEF Materials & Chemistry, N-7465, Trondheim, Norway.

0142-727X/$ - see front matter © 2005 Elsevier Inc. All rights reserved.
doi:10.1016/j.ijheatfluidflow.2005.04.006

review of Raupach et al. (1991), the particle image velocimetry (PIV) investigations of Nakagawa and Hanratty (2003) and by the experiments of Schultz (2000). However, studies of Krogstad et al. (1992), Krogstad and Antonia (1999), Djenidi et al. (1999) and Smalley et al. (2002) showed that the large-scale organized structures present several structural differences between smooth- and rough-wall boundary-layers. The large-scale motions seem to be closer to isotropy and the coherent structures, that are the main source of Reynolds shear stress, appear to have higher average inclination and shorter longitudinal length compared to the smooth-wall case, cf. e.g. Krogstad and Antonia (1994). Moreover, influence of roughness on the small-scale turbulence in the outer layer has been observed by Shafi and Antonia (1997) in turbulent boundary-layer flow and by Poggi et al. (2003) in turbulent open-channel flow. The validity of Townsend's similarity hypothesis was mainly questioned by these observations (Jiménez, 2004).

Experiments on the structure of turbulent rough-wall channel flows are more scarce than those on the boundary-layers (e.g., Mazouz et al., 1994, 1998; Smalley et al., 2002). Direct simulations of turbulent channel flow with transverse bar roughness were only recently performed by Miyake et al. (2001), Ikeda and Durbin (2002), Leonardi et al. (2003) and Nagano et al. (2004). A common feature of all these simulations was that only one of the channel walls was roughened while the other wall remained smooth. In some of these studies the one-sided roughness was partly motivated by the pioneering experiments of Hanjalic and Launder (1972), in which only one channel wall was purposely roughened in order to produce an asymmetric mean flow field. The asymmetry of the channel configuration in all these studies introduced different *local* friction velocities ($u_\tau \equiv \sqrt{\tau_w/\rho}$; here, τ_w is the wall shear stress on the rough or smooth side and ρ is the fluid density) as well as different outer layer length scales characterizing the smooth or rough side. The symmetry of the present channel configuration, however, makes the variation of the turbulence quantities symmetric around the channel mid-plane and the friction velocities on the two sides will be identical. These symmetry properties may serve as a valuable check on the numerical data obtained from a rough-wall channel flow simulation.

Implicit in the analysis of rough-wall turbulence is the premise that the roughness height is very small compared to the bulk flow dimension such that roughness elements do not function as 'bluff bodies'. According to Jiménez (2004), the roughness height should not exceed 2.5% of the channel half-height in order for the roughness elements to have no direct effect on the outer layer flow. A common characteristic of all previous DNS studies is that the roughness elements are relatively high, typically between 10% and 20% of the channel half-height, h, i.e. the blockage effect is rather substantial.

This article is a continuation of our earlier numerical study of pressure-driven turbulent flow in a rod-roughened channel at Reynolds number based on the mean pressure-gradient $Re_\tau = 400$ (Ashrafian et al., 2004). Attached to both channel walls were square rods which protruded only 0.034 of the channel half-height into the flow and were spaced 7 rod heights ($w = 7r$). This roughness configuration corresponded to the so-called "k-type" laboratory roughness (Raupach et al., 1991). Fig. 1 shows the flow geometry and the corresponding coordinate system. In the view of Nikuradse's classification, the regime of the turbulent flow was at the upper end of the transitionally rough region (Nikuradse, 1933). The magnitude of the bulk Reynolds number, $Re = \overline{U}(2h)/\nu$, for the rough and smooth cases were about 8500 and 13 750, respectively (here, $\overline{U}$ is the bulk streamwise velocity, h, is the channel half-height and ν is the kinematic viscosity of the fluid). Details about the

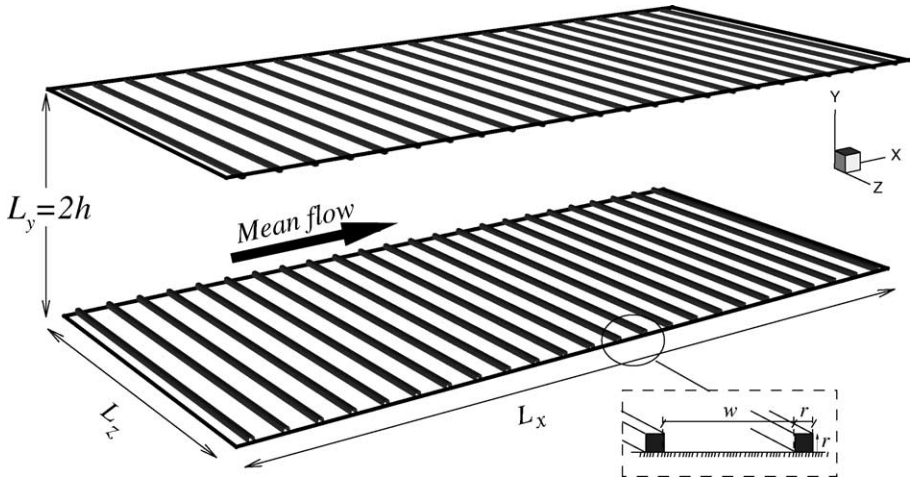

Fig. 1. Symmetric rod-roughened channel geometry and the configuration of the roughness elements and the coordinate system.

grid and the numerical method are given in Ashrafian et al. (2004). In that article, the spatially inhomogeneous layer within which the flow is directly influenced by the individual roughness elements (the roughness sublayer) was carefully examined and the impact of roughness on the mean-velocity profile and the variation of Reynolds stresses outside the roughness sublayer was also studied.

In this article, various turbulence quantities based on the higher-order statistics are obtained from the same DNS of turbulent flow in the rod-roughened channel and compared to those obtained in the simulation of Moser et al. (1999) of a turbulent flow in a smooth cannel at $Re_\tau = 395$. Cross-stream variations midway between the rods will be extensively compared with profiles at mid-crest of the roughness elements. Careful comparisons with experimental data in an identical channel configuration, but at a somewhat higher Re_τ, have been provided elsewhere (Krogstad et al., 2005). Such comparisons could only be made at the particular streamwise location where the hotwire measurements were made, i.e. at mid-crest of the rods.

2. Vorticity field

Vortical motions—as Kücheman (1965) called them *the sinews and muscles of fluid motion*—constitute important features of turbulent flows both at the large energy-producing and the small energy-dissipating scales. In particular, it is expected that any difference in the large-scale motion between rough and smooth-wall layers should be reflected in the vorticity statistics. Krogstad and Antonia (1994) reported approximations to the r.m.s. of vorticity fluctuations ω_i' in the wall-normal and spanwise directions in their study of turbulent boundary-layers over mesh-screen roughness (here, i indicates the direction: x for the streamwise, y for the wall-normal, and z for the spanwise direction). Shafi and Antonia (1997) measured the same quantities in a similar flow using a four-hot-wire vorticity probe in which the effect of spatial resolution of the probe was corrected. They observed that the vorticity variances were slightly larger than those over a smooth wall in the outer layer; thereby suggesting structural differences between the two flows.

Fig. 2 shows the variation of the r.m.s. vorticity fluctuations normalized by u_τ^2/ν for the rough and smooth channels. The variations are similar for both cases in the outer layer. Away from the wall, the three components of the fluctuating vorticity collapse and attain the same magnitude as in the smooth channel. This indicates that in the outer region, the structure of vortical motions are about the same over the rough and smooth walls. Near the walls, however, anisotropy arises rapidly near the smooth wall where large-scale vortices are dominant.

In Fig. 3, the two-dimensional distributions of three components of the r.m.s. vorticity are shown. Here, the bulk flow is from left to right. As it is observed from Fig. 3(a), ω_x is small within the recirculating region behind the rods whereas it attains a maximum just upstream of each rod. Contours of ω_x show vortical structures that are tilted away from the wall due to the collision with the upstream edge of the roughness elements. The streamwise vorticity is also high at the crest of the roughness elements where it creates the maximum reduction in the streamwise Reynolds stress and

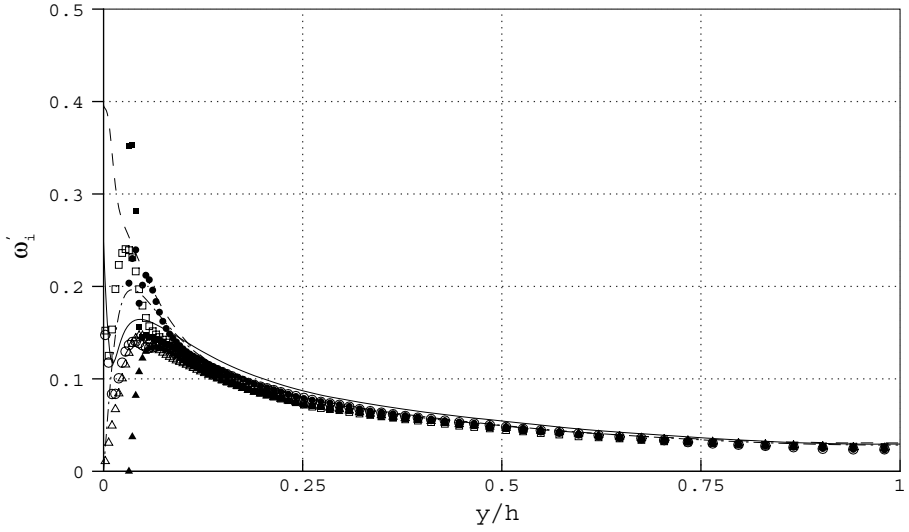

Fig. 2. Root mean square of the vorticity fluctuations in outer coordinates, normalized by u_τ^2/ν. Symbols represent the rough and lines represent the smooth-channel data (Moser et al., 1999). ○, solid line: ω_x; △, – · – · –: ω_y; □, – – –: ω_z. Open symbols: mid-cavity data, filled symbols: mid-crest data.

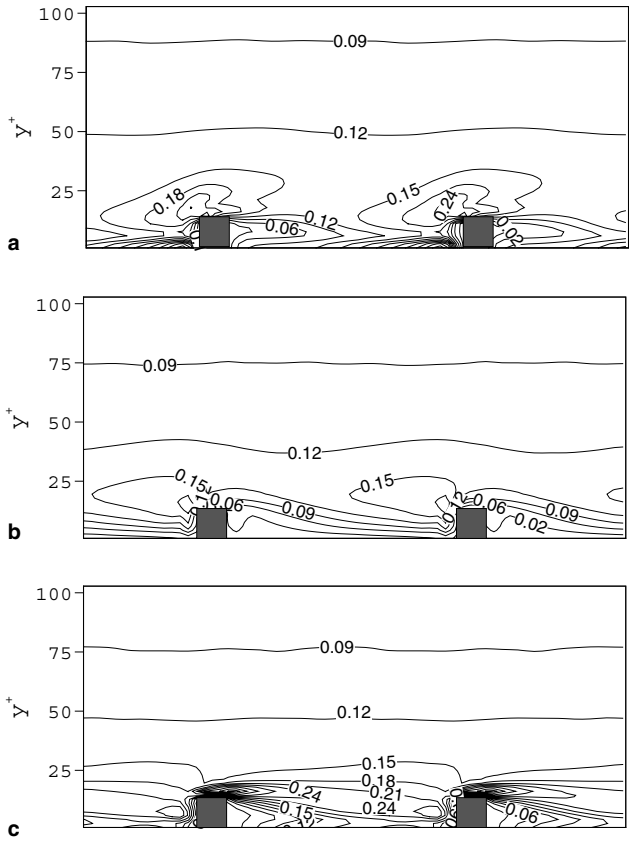

Fig. 3. The two-dimensional distributions of the normalized r.m.s. vorticities near the rough wall. (a) Streamwise, ω_x; (b), wall-normal, ω_y; and (c) the spanwise, ω_z components.

significant dissipation of turbulent kinetic energy (not shown here). Contours of the spanwise r.m.s. vorticity demonstrate an intense shear layer emanating from the roughness crest into the cavity region. As it will be shown later, the motions in this shear layer are responsible for most of the production and dissipation of the turbulent kinetic energy. The wall-normal r.m.s. vorticity, ω_y, has a peak region at the leading edge of the roughness elements. The attached vortices are intensified by vortex stretching due to the high strain at the upstream corner of the rods. In addition to the blocking effect of the transverse rods on the two-dimensional mean flow, this vortical motion produces the spanwise velocity fluctuations near the rods' leading edge.

Fig. 4 shows the iso-surfaces of the streamwise vortices in the rough and smooth channels. Here, and in the rest of this article, the instantaneous fields for the smooth channel are from a simulation of turbulent flow in a smooth channel at $Re_\tau = 400$ (Ashrafian and Andersson, 2006). In the smooth-wall channel, the vortical streaks are elongated in the streamwise direction. They serve as an energy source in the shear layer near the smooth wall. In the rough-wall channel, in the near-wall region of $y^+ < 50$, ω_x structures are disrupted by the rods. Further away from the rough wall, however, coherent vortical structures similar to those seen in the smooth channel emerge. Quasi-streamwise vortical structures are created in the roughness sublayer and lifted away from the wall at angles relatively larger than over a smooth wall. The coherence of the vortices spans over at least two consecutive rods in the streamwise direction. In the spanwise direction, however, these vortices are completely unorganized. Roughness elements cause additional eddies to be formed, consuming mechanical energy and resulting in a higher resistance to the flow.

3. Local anisotropy

In the study of turbulence structures, the Reynolds stress anisotropy has always been of interest by virtue of several reasons. One practical advantage of perusing the Reynolds stress anisotropy tensor is that the problem of having to determine the friction velocity, which matters in experiments, is avoided. Secondly, the Reynolds stress anisotropy is important in the context of developing turbulence models, and finally, it provides useful data in determining the sensitivity of the turbulence structure to different conditions at the wall.

The normalized Reynolds stress anisotropy tensor

$$b_{ij} = \frac{\langle u_i u_j \rangle}{\langle q^2 \rangle} - \frac{1}{3}\delta_{ij}$$

provides a measure of local anisotropy in terms of Reynolds stresses. Here, $\langle q^2 \rangle = \langle u_\ell u_\ell \rangle$ and δ_{ij} is the Kronecker delta. The indices i, j are 1, 2, 3 for the streamwise, wall-normal and spanwise directions, respectively. A summation is understood for repeated indices. b_{ij} is a symmetric and traceless tensor, bounded by $-1/3 \leqslant b_{ij} \leqslant 2/3$ and equal to zero for isotropic turbulence.

Previous anisotropy investigations in boundary-layer flow over rough and smooth walls (Shafi and Antonia, 1995; Djenidi et al., 1999; Antonia and Krogstad, 2001; Mazouz et al., 1998) have revealed that compared to that in the smooth case, the anisotropy in the rough wall boundary-layer is reduced throughout the layer. Data also reflected the ability of the roughness to distribute the turbulent energy more evenly among the three velocity fluctuations. Mazouz et al. (1998) measured the turbulence intensities in a smooth and rough channel roughened by k-type rod roughness. Their data indicated that wall roughness increases the magnitude of the wall-normal component b_{22} across the whole channel. Data of Shafi and Antonia (1995) for a rough-wall turbulent boundary-layer exhibited the opposite trend of the roughness effect on b_{22}. Smalley et al. (2002) examined several data sets from previous rough-wall boundary-layer experiments. Among these was that of Krogstad and Antonia (1999) for a rough-wall bound-

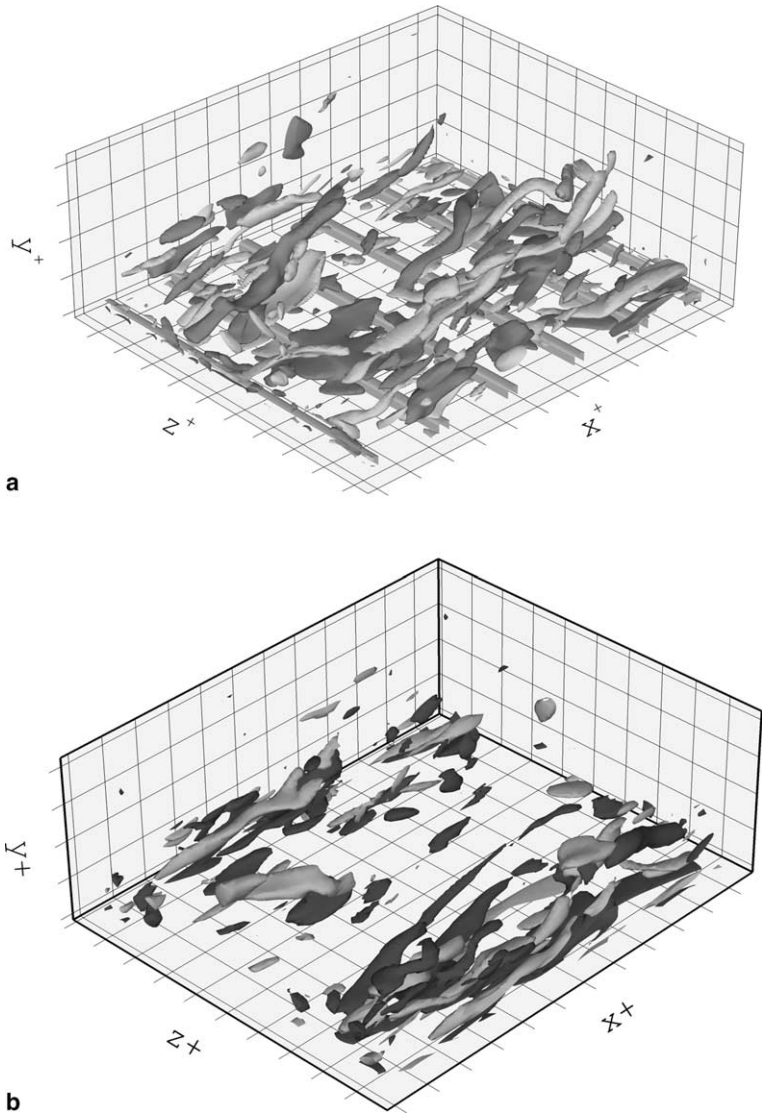

Fig. 4. Iso-surfaces of the streamwise component of the normalized vorticity fluctuations in the (a), rough and (b), smooth channel. The flow direction is rightward. Tick marks on each axis are 50 wall units apart. Black and gray represent positive and negative values, respectively. The iso-surfaces correspond to $\omega_x = \pm 0.25|\omega_x|_{\max}$ in both figures where $|\omega_x|_{\max}$ is the maximum magnitude of the vorticity in each case.

ary-layer on two-dimensional rods with height of only 1.6 mm and pitch-to-height ratio of 4 at a Reynolds number of $Re_\theta = 4806$. Smalley et al. (2002) also investigated the DNS data of a turbulent flow at $Re_\tau = 180$ in a straight channel with one smooth and one rough side, roughened by relatively large two-dimensional rods with heights equal to one-tenth of the channel half-height and pitch-to-height ratio equal to 2 and 5 (*d*- and *k*-type, respectively). They observed, inter alia, that the magnitude of the diagonal components of b_{ij} are all reduced over the *k*-type rod roughness in almost the entire layer for both boundary-layer and channel flows. They also observed that the state of turbulence within the cavity region between two roughness elements is very different from that observed in the near-wall region of a canonical turbulent channel flow.

The variation of b_{ij} in the smooth and rough channels is shown in Fig. 5 in wall coordinates. As can be seen from the b_{11} distribution, strong anisotropy arises in b_{11} through the near-wall behavior of $\langle u^2 \rangle$ on the smooth wall. Near the rough wall, the anisotropy is reduced within the roughness sublayer but remained unchanged further out. The so-called structure parameter $-b_{12}$ (Townsend, 1961) is constant and close to 0.15 in the logarithmic layer both in the rough and smooth channel.

Lumley (1978) proposed a more convenient method for comparing the overall anisotropy. He employed the second (II_b) and third (III_b) principal invariants of the Reynolds stress anisotropy tensor (the first invariant, $I_b \equiv b_{ii}$, is zero). A cross plot of $-II_b$ versus III_b forms an anisotropic invariant map (AIM) where the

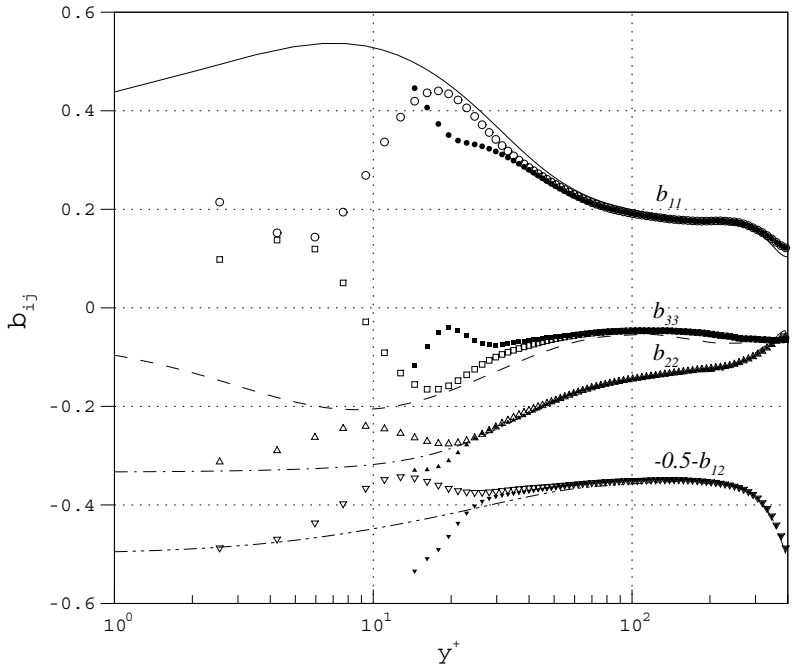

Fig. 5. Components of the Reynolds stress anisotropy tensor. Open and filled symbols represent the rough-channel data at mid-cavity and mid-crest streamwise cross sections, respectively. Lines represent the smooth-channel data (Moser et al., 1999).

second invariant (always negative), II_b, represents the degree of the anisotropy, and III_b indicates the nature of the anisotropy. For a two-dimensional channel flow, $-II_b$ and III_b can be simplified to $-II_b = b_{33}^2 - b_{11}b_{22} + b_{12}^2$ and $III_b = b_{33}^3 + b_{33}II_b$. Fig. 6 shows the AIMs obtained from the smooth-wall and the rough-wall b_{ij} data, together with the AIM boundaries. All possible states of turbulence occur within the bounds of the AIM. The map therefore, clearly highlights any possible changes to the state of turbulence in different regions of the flow. In case of the rough-wall channel, two AIMs are plotted in the figure, corresponding to two streamwise cross sections: mid-cavity and mid-crest.

For three-dimensional isotropic turbulence $-II_b$ and III_b are zero. The left and right curved boundaries of the AIM are defined by $A = \frac{1}{2}III_b(-II_b/3)^{-3/2}$ in which the parameter A indicates the two types of axisymmetric turbulence, i.e., the "disk-like" ($A = -1$) and the "rod-like" ($A = 1$) turbulence. These two types of axisymmetric turbulence correspond to cases in which the

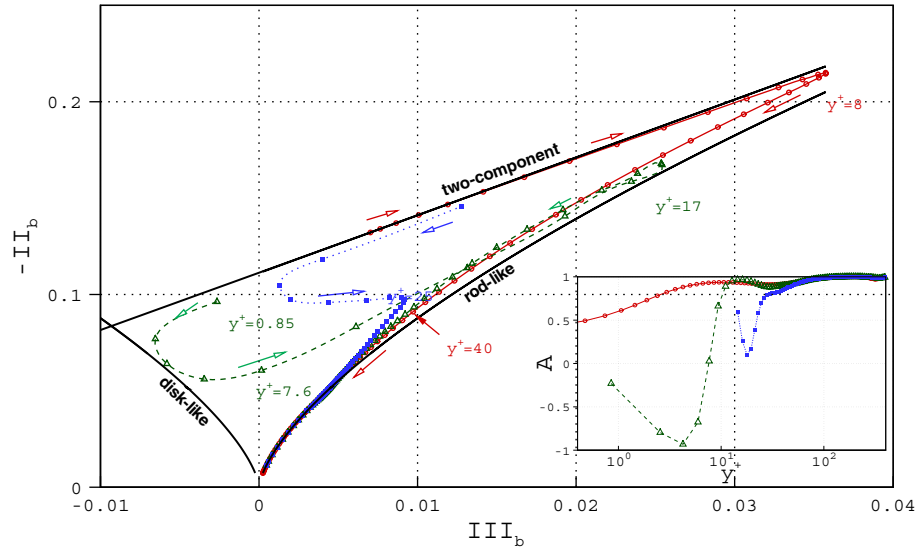

Fig. 6. The anisotropy invariant map for the rough and the smooth cases. Solid line with circles: smooth-channel data (Moser et al., 1999). Dashed line with triangles: rough-wall data from the mid-cavity cross section. Dotted line with filled square: rough-wall data from the mid-crest cross section. The inset represents the variation of parameter A.

magnitude of one diagonal component of the Reynolds stress tensor is much smaller (disk-like) or much greater (rod-like) than the two other components which are identical. The upper straight boundary is defined by the line $0 = 1 + 9II_b + 27III_b$ and represents a two-component state of turbulence.

In Fig. 6, the AIM curve of the smooth-channel DNS data starts from the two-component turbulence limit, as the wall-normal Reynolds stress is forced to zero because of the impermeability condition at the solid wall. The curve reaches a maximum of both $-II_b$ and III_b at $y^+ \approx 8$ (indicated on the map) where $\langle u^2 \rangle$ is the largest of normal stress components. This corresponds to the region of maximum stress anisotropy in the near-wall region. Within the inner region of the smooth-wall layer ($5 < y^+ < 50$), $\langle u^2 \rangle \gg \langle v^2 \rangle$ and $\langle w^2 \rangle > \langle v^2 \rangle$, and the curve follows the right boundary which is the rod-like turbulence limit. The vortical structures near the edge of the viscous sublayer are extended in the streamwise direction and resemble a rod-like turbulence. In the rough wall case, for the mid-cavity cross section, the curve starts from a limit of two-component turbulence and, quite opposite to the smooth-wall case, it proceeds towards the limit of the disk-like turbulence within the cavity region. This can also be seen from the inset of Fig. 6 where the function A is plotted versus y^+. Outside the cavity region, the turbulence rapidly approaches to the rod-like state, similar to that of the smooth-wall turbulence, as the curve approaches the right boundary ($y^+ \approx 17$). The reduced maximum values of $-II_b$ and III_b indicate reduction of anisotropy due to the roughness. The curve collapses to that of the smooth channel in the outer layer region. This is yet another indication of similarity in the outer layer turbulence. Even the data at mid-crest rapidly collapses to the smooth-channel curve without having an extended branch along the right boundary. This observation is most likely associated with the local truncation of streamwise streaks by the crest of the roughness elements.

Another measure of the overall anisotropy of the Reynolds stress tensor is given by the anisotropy function $F = 1 + 9II + 27III$ (Lumley, 1978), which quantifies the approach to either two-dimensional turbulence ($F = 0$) or a three-dimensional isotropic state ($F = 1$). Fig. 7 shows this function for the rough channel, compared with the DNS smooth-channel data. The figure is plotted using inner scaling. The maximum value of F occurs at the channel center, where $F = 0.94$ for the smooth and $F = 0.92$ for the rough case. A range of almost constant F is observed in the interval $50 < y^+ < 250$, thereby indicating similarity in the log-law region of the layers over the two surfaces. The rough-wall profile of F at the mid-cavity cross section departs from that of the smooth case about $y^+ = 20$. The degree of anisotropy is significantly reduced near and within the cavity region. The profile of F at the mid-crest cross section crosses the smooth-channel curve at $y^+ \approx 20$. The turbulence above the crest (i.e. $20 \leqslant y^+ \leqslant 30$) is thus closer to isotropy than that near a smooth wall. This qualitative difference vanishes outside the roughness sublayer.

The present data indicate that the rod roughness in the channel significantly reduces the anisotropy of turbulence structures within the roughness sublayer whereas that of the large-scale structures in the outer layer remains unaffected by the roughness. This observation is rather different from the findings of Krogstad and Antonia (1994) and Shafi and Antonia (1995) in a turbulent boundary-layer on rough walls suggesting a reduction in anisotropy across the whole boundary-layer thickness.

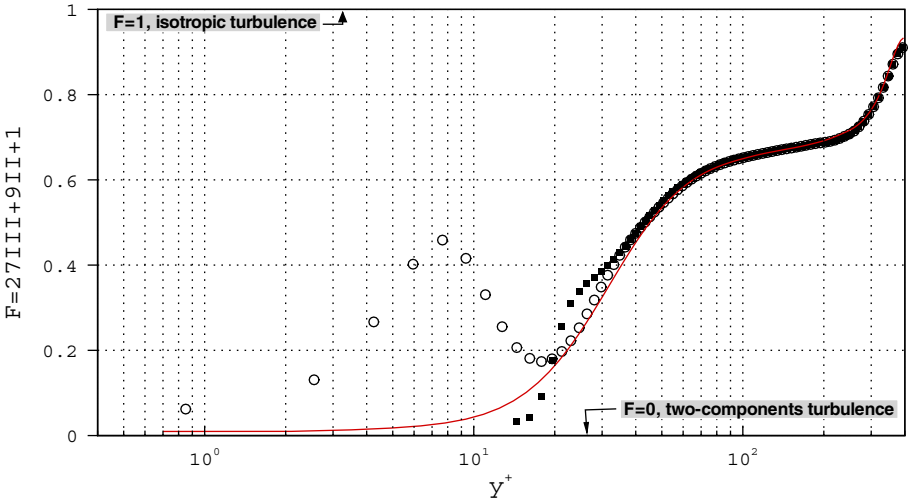

Fig. 7. The invariant F. Open and filled symbols represent the rough-channel data at the mid-cavity and mid-crest streamwise cross sections, respectively. The line represents the smooth-channel data (Moser et al., 1999).

4. Turbulent transport process

The validity of Townsend's similarity hypothesis demands that all the moments of the velocity fluctuations ought to have similar variations in the outer layer. Due to their higher degree of nonlinearity, third-order velocity moments are more sensitive to changes in the structure of turbulence. Smalley et al. (1998) measured the distribution of third-order moments of the velocity fluctuations in a boundary-layer over a wall roughened by two-dimensional circular rods with 4 mm in diameter, operating at $Re_\theta = 4810$ and observed distinct differences below $y/\delta \approx 0.6$ where δ is the boundary-layer thickness. They observed differences not only between the rod-roughened wall and the smooth wall, but also between the rod-roughened wall and other rough walls, viz., a wire mesh and sand grain roughness. The characteristic loss of turbulent kinetic energy (hereinafter denoted TKE) by diffusion exhibited in the wall region over most rough surfaces contrasted with the gain observed over the rod-roughness. Antonia and Krogstad (2001) also investigated a similar behavior above their smaller roughness elements (1.6 mm diameter circular rods at $Re_\theta = 12000$). They recognized that the transport of turbulent energy and momentum flux is towards the wall over the two-dimensional roughness, in contrast with a transport away from the wall over three-dimensional roughness.

In this section, we examine the skewness of the velocity fluctuations, the transport equation of the turbulent kinetic energy and the third-order moments of velocity fluctuations in order to detect any discernible effect of roughness on the structure of the outer layer.

The skewness of the velocity component u_i is defined as $S_{u_i} \equiv \langle u_i^3 \rangle / u_i'^3$ where u_i' is the r.m.s. of the fluctuating velocity u_i. Fig. 8 shows the skewness of the three fluctuating velocity components, viz., S_u, S_v, S_w. The skewness of the spanwise fluctuations, S_w, should be zero everywhere because of the reflection symmetry of the Navier–Stokes equations. The vanishingly small values of the computed S_w is an indication of the adequate sample size for these higher-order statistics. The sampling of the smooth DNS data seems, however, to be less sufficient close to the channel mid-plane. The location of the roughness crest and the approximate thickness of the roughness sublayer (i.e., $5r^+ \approx 68$) are indicated.

Outside the roughness sublayer the collapse of the curves for the smooth- and rough-wall channels is striking. The difference in the S_u curves for the rough and smooth cases is discernible up to $y^+ \approx 90$, i.e. somewhat beyond the estimated roughness sublayer thickness. However, beyond $y^+ = 90$ the collapse is evident. For S_v there is perfect collapse between the smooth- and the rough-wall channel data beyond $y^+ \approx 40$. This collapse of smooth- and rough-channel data for S_v indicates that the large-scale structures in the outer region are similar in the two cases and there is no distinct difference in the wall-normal turbulence transport in the outer layer. However, the plot clearly shows that the structure of the large-scale wall-normal energy-carrying motions within the roughness sublayer is strongly affected by the roughness. The streamwise skewness changes sign from negative to positive values at about $y^+ \approx 12$ in the smooth case, whereas in the rough case, the sign-change occurs at $y^+ \approx 25$. For the smooth case, the sign change for S_v occurs at about $y^+ \approx 33$ and again

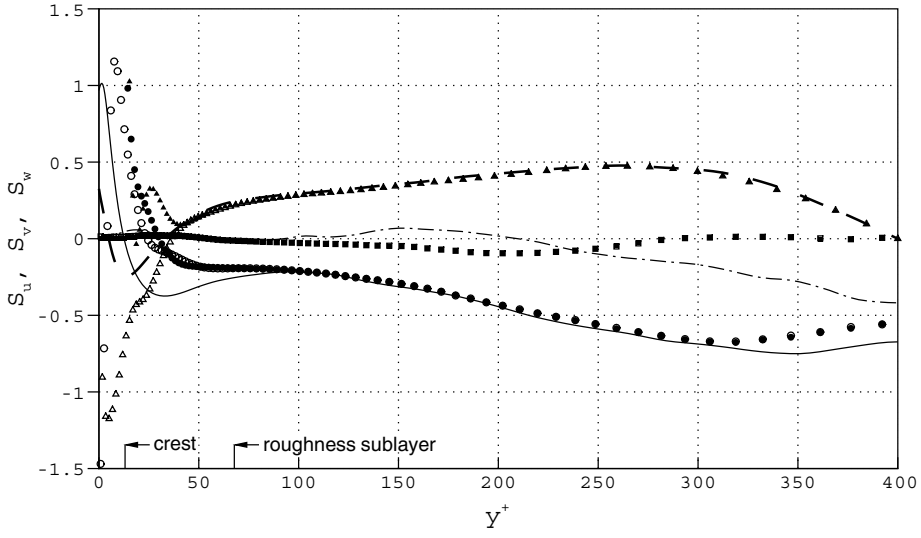

Fig. 8. Skewness of the components of the fluctuating velocity. Open and filled symbols represent the rough-channel data at the mid-cavity and mid-crest streamwise cross sections, respectively. Lines represent the smooth-channel data (Moser et al., 1999). ○, solid line: S_u; △, – – –: S_v; □, – · – · –: S_w.

just about the edge of the viscous sublayer ($y^+ \approx 5$). For the rough case and at the mid-cavity cross section the sign change for S_v occurs at $y^+ \approx 40$. These results imply that strong sweep motions ($u > 0$, $v < 0$) are the dominant events inside the roughness sublayer region and contribute significantly to the near-wall flow structure over the rod roughness. The contribution of sweep motions to the turbulent shear stress is largest just above the cavity. This is in agreement with the observation of Grass et al. (1993) who investigated energetic inrush events towards the wall with k-type strip roughness and also with the results from the rough-wall boundary-layer experiment of Bisceglia et al. (2001) on two-dimensional circular rod roughness.

The transport equation for the TKE, $k \equiv \frac{1}{2}\langle q^2 \rangle$, is

$$\left(\partial_t + \langle U_\ell \rangle \partial_\ell - \nu \nabla^2\right) k + \partial_\ell \left(\frac{1}{2} \langle u_i u_i u_\ell \rangle + \frac{1}{\rho} \langle p u_\ell \rangle \right) = P_k - \epsilon, \tag{1}$$

where $P_k \equiv -\langle u_i u_\ell \rangle \partial_\ell \langle U_i \rangle$ is the local production rate, and $\epsilon \equiv \nu \langle (\partial_j u_i)^2 \rangle$ is the viscous dissipation rate of the TKE. The first term on the left-hand side of Eq. (1) (hereinafter denoted by C) can be interpreted as the net change of k by advection (in the lateral and streamwise directions) and by viscous diffusion. Since the flow under consideration is statistically steady, $\partial_t k = 0$. The second term on the left-hand side of Eq. (1) can be interpreted as the net energy gain from the lateral and streamwise flow of energy by fluctuations of velocity and pressure. This term (hereinafter denoted by Φ), is a summation of the turbulent transport and pressure diffusion.

Fig. 9 shows the different terms in the budget equation (1) in wall coordinates at the mid-cavity location and the corresponding data for the smooth wall. All terms are normalized by u_τ^4/ν. Locations of the roughness crest and the edge of the estimated roughness sublayer are indicated in the figure. No discernible difference between the rough and the smooth channel is observed in the outer layer, i.e. beyond $y^+ \approx 68$. The dissipation rate is maximum just at the plane of the roughness crest due to the intense shear layer emanating from the roughness crest. The magnitude of the maximum dissipation is, however, reduced compared to that of the smooth wall. A pronounced increase in the maximum production rate is observed at $y^+ \approx 20$. The peak production in the smooth case is at $y^+ \simeq 12$. The difference between these two peak positions is only about half of the rod height. Compared to the smooth case, the magnitude of the viscous diffusion term was noticeably smaller (not shown here). The Φ-term has a similar trend as that over the smooth wall except that its magnitude is more pronounced in the roughness sublayer than in the smooth case. The roughness sublayer is certainly not in an energy equilibrium state, i.e., $P_k \neq \epsilon$.

Antonia and Krogstad (2001) reported that surface roughness has a major impact on the magnitude and direction of the turbulent transport process, i.e. the sign of the term $\partial_\ell \left(\frac{1}{2} \langle u_i u_i u_\ell \rangle \right)$. In order to examine the relevance of this observation in the present case, the variation of the wall-normal transport of the Reynolds stresses are shown in Fig. 10 by plotting the associated normalized third-order moments $\langle u^2 v \rangle$, $\langle v^3 \rangle$, $\langle w^2 v \rangle$ and $\langle u v^2 \rangle$. All data collapse sufficiently well with the smooth-channel results

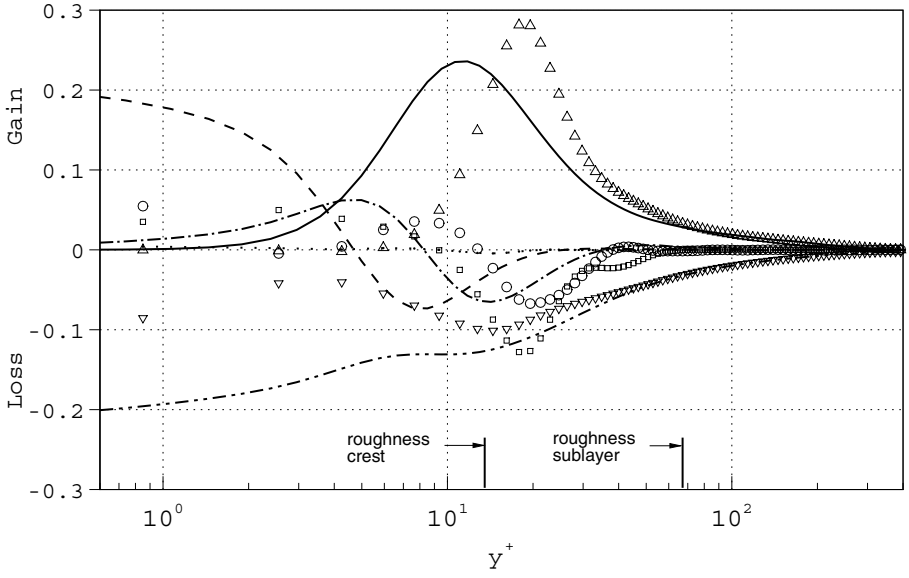

Fig. 9. Normalized budget of TKE ($0 = -C - \Phi + P_k - \epsilon$) at the mid-cavity cross section. Symbols represent the rough and lines represent the smooth-channel data (Moser et al., 1999). ○, – – – –: $-C$; □, – · – · –: $-\Phi$; △, solid line: P_k; ▽, – · · – · · –: $-\epsilon$; · · · · ·: residue of the rough-wall channel data.

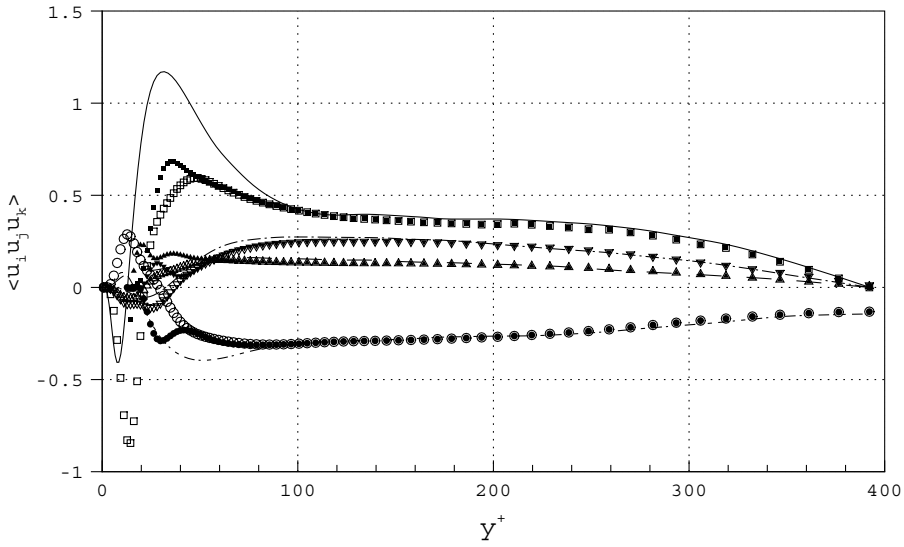

Fig. 10. Third-order fluctuating velocity moments normalized by u_τ^3. Open and filled symbols represent the rough-channel data at the mid-cavity and mid-crest streamwise cross sections, respectively. Lines represent the smooth-channel data (Moser et al., 1999). ○, and – · · – · · –: $\langle uv^2\rangle$; □ and the solid line: $\langle u^2v\rangle$; △, – – – : $\langle w^2v\rangle$; ▽, – · – · –: $\langle v^3\rangle$.

for $y^+ > 100$, whereas there are major differences in $\langle u^2v\rangle$ and $\langle uv^2\rangle$ for $y^+ < 100$. This indicates that roughness strongly affects the transport process of the normal stress $\langle u^2\rangle$ and shear stress $\langle uv\rangle$ in the inner layers. At the plane of roughness crests, both components show an increase in magnitude midway between the rods. Just above the roughness crest, however, their magnitudes are significantly reduced.

The roughness sublayer is a non-equilibrium shear layer where strong inhomogeneities are present, especially in the vicinity of the roughness elements (Ashrafian et al., 2004). Therefore, the turbulent transport term in the TKE balance equation (1) also contains contributions to the TKE transport in the wall-parallel directions. In order to examine the effect of roughness on the transport of TKE only in the wall-normal direction, the wall-normal TKE transport velocity, V_k, is defined by the ratio of the wall-normal turbulent transport of TKE to the magnitude of TKE itself, i.e. $V_k \equiv \langle vu_\ell u_\ell\rangle/\langle u_\ell u_\ell\rangle$. V_k is a quantity with dimension of velocity and measures the velocity with which the TKE is transported by the turbulence either toward ($V_k < 0$) or away from ($V_k > 0$) the wall.

Fig. 11 shows that this characteristic velocity is strongly affected by the roughness in the near-wall region. The effect of roughness extends up to $y^+ \approx 100$. However, in the outer layer the effect of roughness on the wall-normal turbulent transport is virtually negligible. The figure also shows a substantial wall-ward transport of the TKE at the mid-cavity cross section for $y^+ \leqslant 22$, i.e. below the position of maximum production of the TKE. On the contrary, no wall-ward transport takes place just above the rods.

5. Turbulence structures

From the various averaged quantities presented in the preceding sections, we showed that an equilibrium layer (with nearly constant Reynolds stress anisotropies and production–dissipation balance) exists only outside the roughness sublayer and thus supports the outer-layer similarity between the turbulence in smooth- and rough-wall channels. Within the roughness sublayer, however, the turbulence is less structured and in a non-equilibrium state so that the near-wall behavior of many flow properties are considerably changed. This section is devoted to the study of the characteristics associated with various instantaneous fields within the roughness sublayer.

Fig. 12 portrays a snapshot of the instantaneous TKE in an arbitrary (x–y) plane covering a large proportion of the flow field in the smooth and rough cases. Darker regions are associated with greater magnitude of the turbulent kinetic energy. Near the rough wall, vigorous motions are seen in the layers just above the plane of roughness crests. Eddies are shed from the roughness elements and convected downstream with the mean flow. The coherence of these eddies in the streamwise direction is disrupted by the roughness elements. Lumps of high-speed fluid seem to interact with the roughness elements and then break up. Large volumes of intense velocity fluctuations are formed outside the roughness sublayer and convected downstream with the mean flow and can even reach the channel center line. The smooth wall is relatively inactive, except near the wall wherestreaks with considerable streamwise coherence exist.

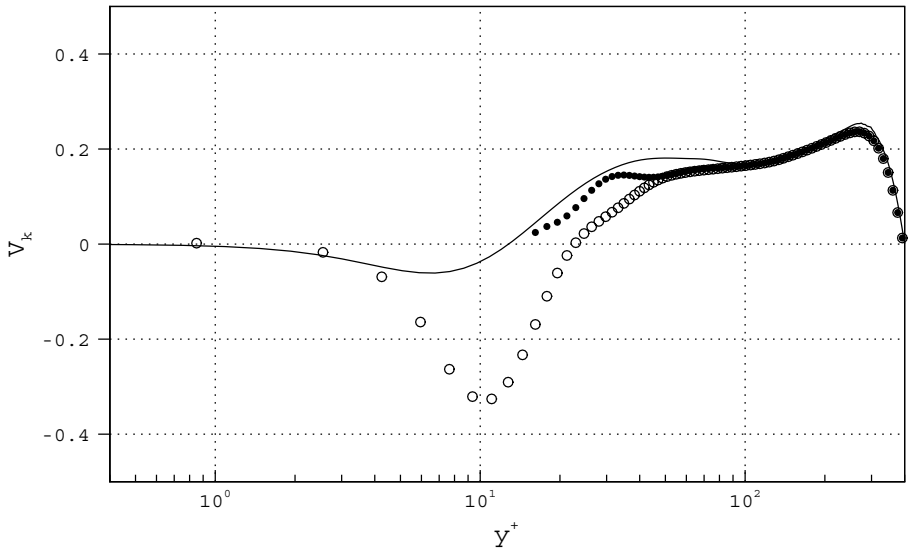

Fig. 11. The wall-normal TKE transport velocity V_k. Open and filled symbols represent the rough-channel data at the mid-cavity and mid-crest streamwise cross sections, respectively. The line represents the smooth-channel data (Moser et al., 1999).

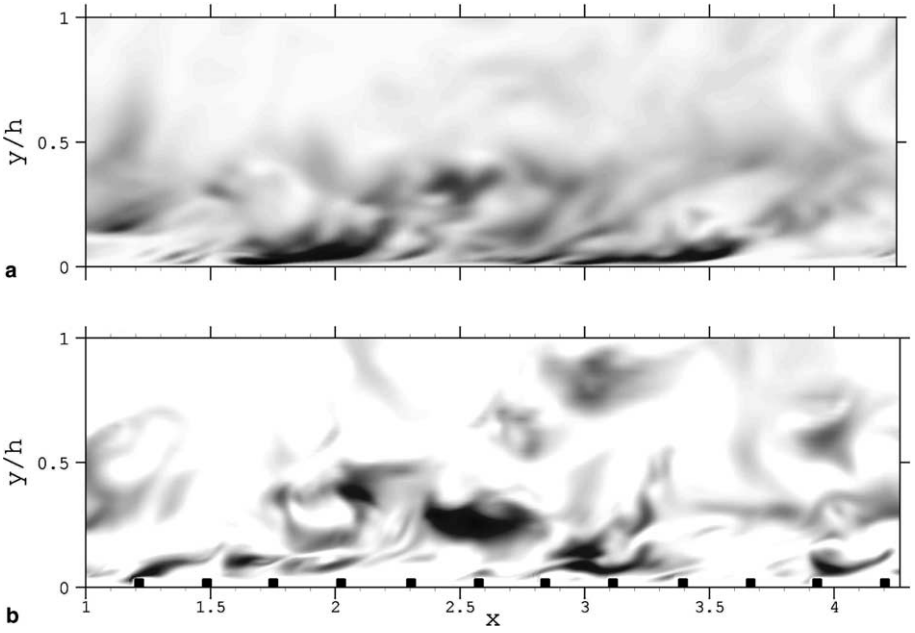

Fig. 12. The instantaneous turbulent kinetic energy in (a) the smooth (Ashrafian and Andersson, 2006) and (b) rod-roughened channels. The mean flow direction is from left to right.

Ashrafian et al. (2004) observed that streaky structures of u-fluctuations, similar to the smooth case, also exist over the rough wall but with significantly reduced coherence in the streamwise direction and no obvious spanwise coherence. The credibility of this result is further examined here. From Section 4 we recall that above the roughness, the TKE production reaches its maximum at $y^+ \approx 18$ whereas in the smooth case, the TKE production peaks at $y^+ \approx 12$. Fig. 13 shows contour plots of the wall-normal component of the fluctuating vorticity, ω_y, in the xz-plane of maximum TKE production. Compared to the smooth case, the organization of the contours of constant ω_y is severely reduced near the rough wall.

Flow visualizations of the roughness sublayer suggest that roughness reduces the large-scale flow structure within the roughness sublayer. In order to investigate the effect of roughness on small-scale structures, the

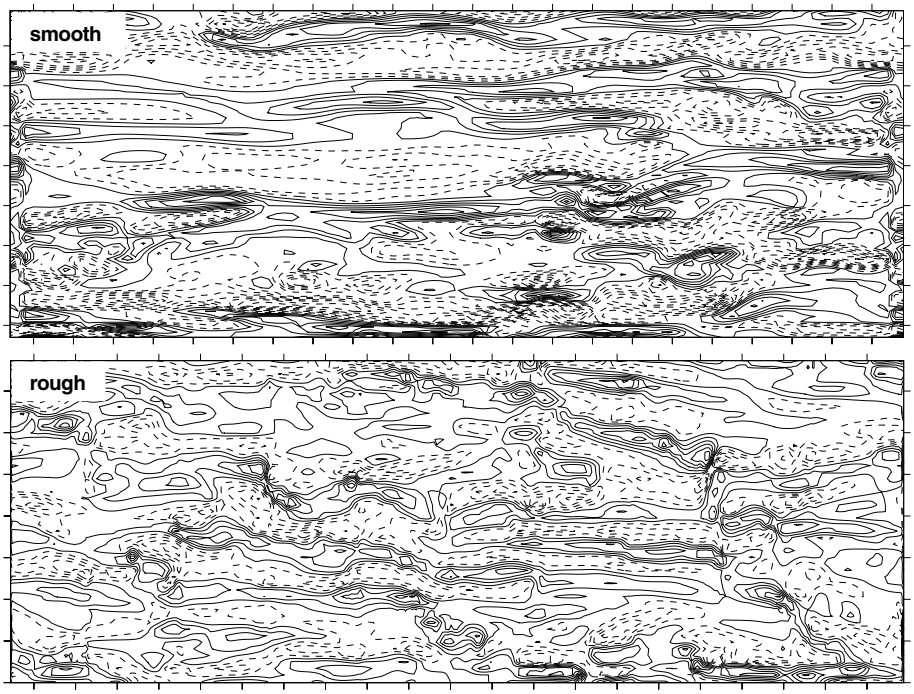

Fig. 13. Structure of instantaneous normalized ω_y at the plane of maximum TKE production in the smooth ($y^+ \simeq 12$) and rough channel ($y^+ \simeq 18$). The mean flow direction is from left to right, and tick marks denote 50 wall units.

Taylor micro-scale is employed. The Taylor micro-scale in the x_j direction for the u_i velocity fluctuation, $\lambda(u_i; x_j)$, is defined as

$$\lambda(u_i;x_j) = u_i'\left\langle \left(\frac{\partial u_i}{\partial x_j}\right)^2 \right\rangle^{-1/2}$$

where u_i' is the r.m.s. of fluctuating velocity component i (the summation rule on the index i is not applied). The Taylor micro-scale is obtained from the r.m.s. u_i and the fluctuating strain rate, $\partial u_i/\partial x_j$ and contains information from the small scale turbulence. Since λ can be related to the two-point velocity correlations (see Pope, 2000, p. 198), the various correlation lengths in the xy-plane can also be inferred therefrom.

Figs. 14 and 15 compare the rough- and smooth-wall distributions of Taylor micro-scales in the streamwise and spanwise directions, respectively. Both the axes are normalized by $\delta_v = \nu/u_\tau$ and the abscissa is logarithmic in order to emphasize the wall region. It can be observed that roughness has no effects on the small scale structures outside the roughness sublayer. In Fig. 14, $\lambda(u; x)$ is substantially reduced within the roughness sublayer region, in accordance with the comparison of ω_y-fluctuations near rough and smooth walls in Fig. 13. The local maximum of $\lambda(u; x)$ near the smooth wall is at $y^+ \simeq 5$, i.e., near the edge of the viscous sublayer. Above the rough wall this local maximum has vanished completely. In the spanwise direction, $\lambda(v; z)$ in Fig. 15 slightly increases within the roughness sublayer and inside the cavity region, whereas on top of the roughness crest, it is significantly reduced. Figs. 14 and 15 suggest that the correlation lengths in the streamwise direction are significantly shortened, however, the correlation lengths in the spanwise direction are only moderately affected by the roughness. It should be noted that a Taylor micro-scale does not directly represent a velocity correlation length. However, λ can reveal the differences in length scales between the smooth- and rough-wall layers.

6. Summary and discussions

Direct numerical simulation of a turbulent flow in a rod-roughened channel has been performed to investigate the effects of surface roughness on the statistical features of mainly large scales of turbulence. The friction Reynolds number, Re_τ, based on the mean pressure-gradient, was 400 and the turbulent flow was in the upper limit of the transitionally rough regime. Owing to the symmetry of the roughened channel, results from the present study (normalized by u_τ) were directly compared to those obtained by Moser et al. (1999) from a smooth-channel flow DNS at $Re_\tau = 395$. Since the driving pressure-gradient was practically the same in the smooth and the roughened channels, the bulk flow rate is lower in the latter. The bulk Reynolds number for the rough and smooth channels, based on the channel height, was about 8500 and 13 750, respectively.

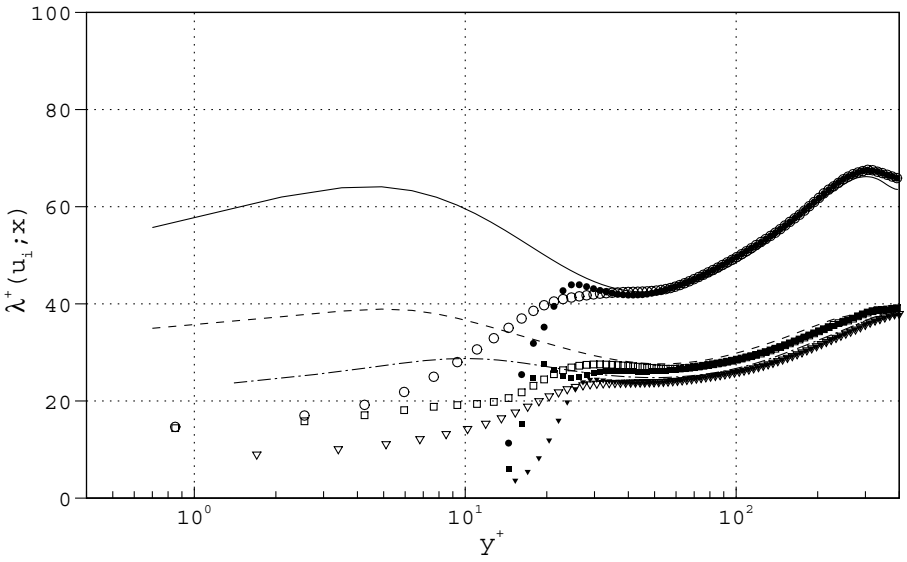

Fig. 14. The Taylor micro-scales in the streamwise direction. Open and filled symbols represent the rough-channel data at the mid-cavity and mid-crest streamwise cross sections, respectively. Lines represent the smooth-channel data (Ashrafian and Andersson, 2006). ○, and solid line: $\lambda^+(u; x)$; □, – – –: $\lambda^+(v; x)$; ▽, – · – · –: $\lambda^+(w; x)$.

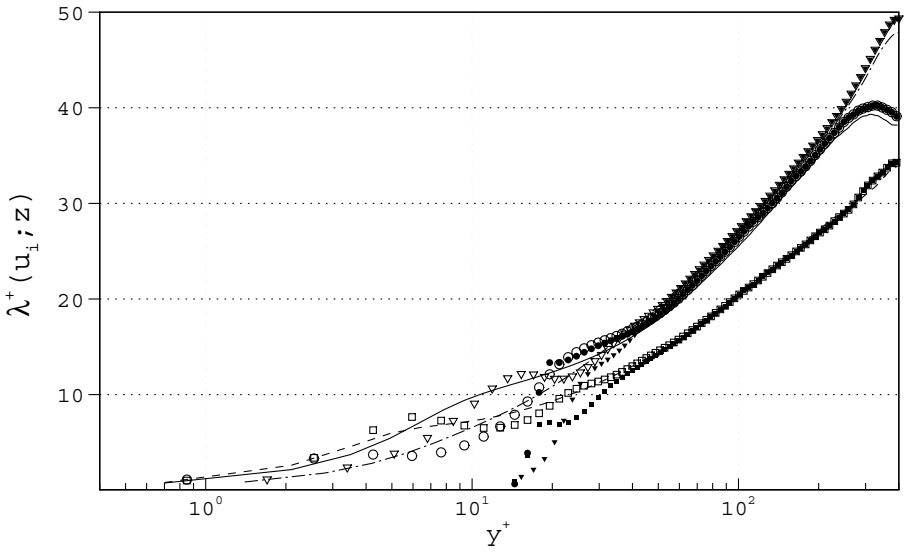

Fig. 15. The Taylor micro-scales in the spanwise direction. Open and filled symbols represent the rough-channel data at the mid-cavity and mid-crest streamwise cross sections, respectively. Lines represent the smooth-channel data (Ashrafian and Andersson, 2006). ○, and solid line: $\lambda^+(u; z)$; □, – – –: $\lambda^+(v; z)$; ▽, – · – · –: $\lambda^+(w; z)$.

The r.m.s. of the vorticity fluctuations were not significantly altered in the outer layer, whereas modifications were observed within the roughness sublayer. The snapshots of the iso-surfaces of the fluctuating vorticity components revealed that the highly disrupted vortical structures near the rough-wall region recover rapidly in the regions away from the roughness elements ($y^+ > 20$) and attain their coherence in form of patterns very similar to what is seen in turbulent flow in a smooth channel. Ashrafian et al. (2004) observed a similar behavior of the low-speed streaks above the rough surface. This implies that as long as sufficiently rapid mean deformation or a significant Reynolds shear stress is sustained, vortical structures and the associated low-speed streaks will be formed. As strongly suggested by the observation of streaks by Lam and Banerjee (1992) near free-slip interfaces, the formation of streaks is independent of the presence of the wall provided that the shear rate is sufficiently high. The numerical experiments of Jiménez and Pinelli (1999) have confirmed that near-wall turbulence is maintained by a cycle which is localized in the region $20 < y^+ < 60$. In the present case, it is likely

that the small roughness elements ($r^+ = 13.6$) have not completely altered the "autonomous cycle" of turbulence generation. Therefore, vortical structures similar to those observed near smooth walls emerged.

The investigation of the Reynolds stress anisotropy revealed that the stress anisotropy is unaffected in the outer layer region although the anisotropy is greatly reduced within the roughness sublayer. Structural differences similar to those reported by Krogstad and Antonia (1994), Krogstad and Antonia (1999) and Shafi and Antonia (1995) in a turbulent boundary-layer over k-type mesh roughness were not observed in the present rough-wall channel flow. The present results can therefore be added to the body of evidence that supports the classical hypothesis of outer-layer similarity of Townsend (1976).

In order to assess the turbulent transport process over the rough walls, the third-order moments of the velocity fluctuations together with the TKE transport equation were analyzed. The perfect collapse between the profiles of S_u and S_v clearly showed that the structure of large-scale energy-carrying motions are similar at $y^+ > 100$. Some discernible differences, however, were observed in the skewness of the u-component of the fluctuating velocity as well as in the third-order moments $\langle u^2 v\rangle$ and $\langle uv^2\rangle$ in the interval $5r^+ < y^+ < 100$. This observation suggests that the thickness of the roughness sublayer depends on which statistical quantity is used to characterize it. For the roughness-induced inhomogeneity influences and effects on the Reynolds stresses, Ashrafian et al. (2004) and many others (see Raupach et al., 1991) reported five times roughness height r^+ as a good approximation of the roughness sublayer thickness. The present study, however, suggests that if based on some higher-order statistics the edge of the roughness sublayer may extend to about eight times the roughness height. The third-order moments of the fluctuating velocity components also show that the wall-normal transport of the TKE is greatly affected by surface roughness. Compared to that over the smooth walls, the magnitude of the characteristic velocity with which the TKE is transported towards the channel center is reduced in the region $20 < y^+ < 100$, whereas a wall-ward velocity transports TKE into the cavities between the rods. The study of Taylor micro-scales outside the roughness sublayer showed no roughness effects on the small-scale turbulence. Within the roughness sublayer, however, the correlation lengths in the streamwise direction are significantly shortened, as expected.

Much of the present results summarized above are in agreement with previous experimental results (mainly in boundary-layers) which suggested that outer-layer similarity between smooth and rough surfaces holds (e.g., Raupach et al., 1991; Grass et al., 1993; Nakagawa and Hanratty, 2003). The following factors may, however, affect the turbulence structure. The geometry of the roughness elements (being two- or three-dimensional) and their arrangement on the walls (e.g. the roughness density) are believed to be important factors in producing different roughness effects. The geometry of the flow itself is another important factor. The geometrical difference between channel and boundary-layer flows, for example, may result in different roughness effects. The free-stream–boundary-layer interface is absent in the channel flow. Instead, the shear layers along the two walls merge at the channel center line. There is also the possibility that inner-region structures from opposite walls do interact. This possibility, which is more likely at low Reynolds numbers, challenges the interpretation of results obtained in experimental and numerical studies in which turbulent flows in asymmetric channels (one wall roughened, one wall smooth) are considered. This study aimed to address some aspects of turbulent flow in a rod-roughened channel, but further investigations of roughness-induced flow phenomena are carefully needed.

Acknowledgements

The authors are grateful to Professor P.-Å. Krogstad (NTNU, Trondheim) for inspiring discussions and useful comments. The Norwegian Research Council is highly acknowledged for the financial support and the grant of necessary CPU time. The computer code MGLET was kindly made available by Professors R. Friedrich (TU München) and H. Wengle (Universität Bundeswehr München).

References

Antonia, R.A., Krogstad, P.-Å., 2001. Turbulence structure in boundary layers over different types of surface roughness. Fluid Dynamics Research 28, 139–157.

Ashrafian, A., Andersson, H.I., Manhart, M., 2004. DNS of turbulent flow in a rod-roughened channel. International Journal of Heat and Fluid Flow 25, 373–383.

Ashrafian, A., Andersson, H.I., 2006. Roughness effects in turbulent channel flow, International Journal of Progress in Computational Fluid Dynamics 6, in press.

Bisceglia, S., Smalley, R.J., Djenidi, L., Antonia R.A., 2001. Structure of rough-wall turbulent boundary layers at relatively high Reynolds number. In: Transactions of the 14th Australasian Fluid Mechanics Conference, pp. 195–198.

Djenidi, L., Elavarasan, R., Antonia, R.A., 1999. The turbulent boundary layer over transverse square cavities. Journal of Fluid Mechanics 395, 271–294.

Grass, A.J., 1971. Structural features of turbulent flow over smooth and rough boundaries. Journal of Fluid Mechanics 50, 233–255.

Grass, A.J., Stuart, R.J., Mansour-Tehrani, M., 1993. Common vortical structure of turbulent flows over smooth and rough boundaries. AIAA Journal 331, 437–447.

Hanjalic, K., Launder, B.E., 1972. Fully developed asymmetric flow in a plane channel. J. Fluid Mech. 51, 301–333.

Ikeda, T., Durbin, P.A., 2002. Direct simulations of a rough-wall channel flow, Report No. TF–81, Department of Mechanical Engineering, Stanford University, Stanford, CA, USA.

Jiménez, J., 1999. The physics of wall turbulence. Physica A 263, 252–262.

Jiménez, J., 2004. Turbulent flows over rough walls. Annual Review of Fluid Mechanics 36, 173–196.

Jiménez, J., Pinelli, A., 1999. The autonomous cycle of near-wall turbulence. Journal of Fluid Mechanics 389, 335–359.

Krogstad, P.-Å., Antonia, R.A., 1994. Structure of turbulent boundary layers on smooth and rough walls. Journal of Fluid Mechanics 277, 1–21.

Krogstad, P.-Å, Antonia, R.A., 1999. Surface roughness effects in turbulent boundary layers. Experiments in Fluids 27, 450–460.

Krogstad, P.-Å., Antonia, R.A., Browne, L.W.B., 1992. Comparison between rough- and smooth-wall turbulent boundary layers. Journal of Fluid Mechanics 245, 599–617.

Krogstad, P.-Å, Andersson, H.I., Bakken, O.M., Ashrafian, A., 2005. An experimental and numerical study of channel flow with rough walls. Journal of Fluid Mechanics 530, 327–352.

Kücheman, D., 1965. Report on the I.U.T.A.M. symposium on concentrated vortex motions in fluids. Journal of Fluids Engineering 21, 1–20.

Lam, K., Banerjee, S., 1992. On the condition of streak formation in a bounded turbulent flow. Physics of Fluids A4, 306–320.

Leonardi, S., Orlandi, P., Smalley, R.J., Djenidi, L., Antonia, R.A., 2003. Direct numerical simulations of turbulent channel flow with transverse square bars on one wall. Journal of Fluid Mechanics 491, 229–238.

Lumley, J., 1978. Computational modeling of turbulent flows. Advances in Applied Mechanics 18, 123–176.

Mazouz, A., Labraga, L., Tournier, C., 1994. Behaviour of the Reynolds stress on rough walls. Experiments in Fluids 17, 39–44.

Mazouz, A., Labraga, L., Tournier, C., 1998. Anisotropy invariant of Reynolds stress tensor in a duct flow and turbulent boundary layer. Journal of Fluids Engineering 120, 280–284.

Miyake, Y., Tsujimoto, K., Nakaji, M., 2001. Direct numerical simulation of rough–wall heat transfer in a turbulent channel flow. International Journal of Heat and Fluid Flow 22, 237–244.

Moser, R., Kim, J., Mansour, N., 1999. Direct numerical simulation of channel flow up to $Re_\tau = 590$. Physics of Fluids 11, 943–945.

Nagano, Y., Hattori, H., Yasui, S., Houra, T., 2004. DNS of velocity and thermal fields in turbulent channel flow with transverse-rib roughness. International Journal of Heat and Fluid Flow 25, 393–403.

Nakagawa, S., Hanratty, T.J., 2003. Influence of a wavy boundary on turbulence. II. Intermediate roughened and hydraulically smooth surfaces. Experiments in Fluids 35, 437–447.

Nikuradse, J., 1933. Strömungsgesetz in Rauhen Röhren. VDI Forschungsheft, no. 361 (English translation (1950) NACA TM 1292).

Perry, A.E., Lim, K.L., Henbest, S.M., 1987. An experimental study of the turbulence structure in smooth- and rough-wall boundary layers. Journal of Fluid Mechanics 177, 437–466.

Poggi, D., Porporato, A., Ridolfi, L., 2003. Analysis of the small-scale structure of turbulence on smooth and rough walls. Physics of Fluids 15, 35–46.

Pope, S.B., 2000. Turbulent Flows. Cambridge University Press, Cambridge.

Raupach, M.R., Antonia, R.A., Rajagopalan, S., 1991. Rough-wall turbulent boundary layers. Applied Mechanics Review 44, 1–25.

Schultz, M.P., 2000. Turbulent boundary layers on surfaces covered with filamentous algae. Journal of Fluids Engineering 122, 357–363.

Shafi, H.S., Antonia, R.A., 1995. Anisotropy of the Reynolds stresses in a turbulent boundary layer on a rough wall. Experiments in Fluids 18, 213–215.

Shafi, H.S., Antonia, R.A., 1997. Small-scale characteristics of a turbulent boundary layer flow over a rough wall. Journal of Fluid Mechanics 342, 263–293.

Smalley, R.J., Antonia R.A., Krogstad, P.-Å., 1998. Turbulent transport of the Reynolds stresses above a rod-roughened boundary layer. In: Transactions of the 13th Australian Fluid Mechanics Conference, pp. 615–618.

Smalley, R.J., Leonardi, S., Antonia, R.A., Djenidi, L., Orlandi, P., 2002. Reynolds stress anisotropy of turbulent rough wall layers. Experiments in Fluids 33, 31–37.

Townsend, A.A., 1961. Equilibrium layers and wall turbulence. Journal of Fluid Mechanics 11, 97–120.

Townsend, A.A., 1976. The Structure of Turbulent Shear Flow, second ed. Cambridge University Press, Cambridge.